High-resolution underway measurements of phytoplankton photosynthesis and abundance as innovative addition to water quality monitoring programs

5 Hedy M. Aardema[1,2], Machteld Rijkeboer[1], Alain Lefebvre[3], Arnold Veen[1], and Jacco C. Kromkamp[4]

[1]Laboratory for Hydrobiological Analysis, Rijkswaterstaat (RWS), Zuiderwagenplein 2, 8224 AD Lelystad, The Netherlands
[2]Department of Climate Geochemistry, Max Planck Institute for Chemistry, Hahn-Meitner-Weg 1, 55128 Mainz, Germany
[3]Ifremer, Laboratoire Environnement et Ressources, BP 699, 62321 Boulogne sur Mer, France
[4]Department of Estuarine and Delta Systems, NIOZ Royal Netherlands Institute for Sea Research and Utrecht University, P.O. box
10 140, 4400 AC Yerseke, The Netherlands

Correspondence to: Hedy M. Aardema (hedy.aardema@mpic.de),

Abstract. Marine waters can be highly heterogeneous both on a spatial and temporal scale, yet monitoring programs are currently
15 relying primarily on low-resolution methods. This potentially leads to undersampling. This study explores the potential of two high-resolution methods for monitoring of phytoplankton dynamics; Fast Repetition Rate fluorometry for information on phytoplankton photosynthesis and productivity and automated scanning flowcytometry for information on phytoplankton abundance and community composition. These methods were tested in combination with an underway Ferrybox system during four cruises on the Dutch North Sea in April, May, June, and August of 2017. The high-resolution methods were able to visualize both spatial and
20 temporal variability of the phytoplankton community in the Dutch North Sea. Spectral cluster analysis was applied to objectively interpret the multitude of parameters and visualize potential spatial patterns. This resulted in the identification of biogeographic regions with distinct phytoplankton communities, which varied per cruise. Our results clearly show that the sampling based on fixed stations does not give a good representation of the spatial patterns, showing the added value of underway high-resolution measurements. To fully exploit the potential of the tested high-resolution measurement set-up, methodological constraints need
25 further research. Among these constraints are; accounting for the diurnal cycle in photophysiological parameters concurrent to the spatial variation, better predictions of the electron requirement for carbon fixation to estimate gross primary productivity, and the identification of more flowcytometer clusters with informative value. Nevertheless, the richness of additional information provided by high-resolution methods can improve existing low-resolution monitoring programs towards a more precise and ecosystemic ecological assessment of the phytoplankton community and productivity.

30

35

KEY WORDS: Fast Repetition Rate fluorometry, flow cytometry, phytoplankton photosynthesis, spatial variability, primary productivity

1 Introduction

The Dutch North Sea is of major socio-economic importance because of its close proximity to densely populated areas and its intensive utilization for shipping, fishing, sand extraction and development of offshore windmill farms. Due to this high anthropogenic pressure, the North Sea has undergone considerable biogeochemical and biological changes in the past decades (Burson et al., 2016; Capuzzo et al., 2015 and 2017). For example, nutrient load and stoichiometry were fluctuating substantially due to the inflow of wastewater and agricultural run-off and subsequent mitigation efforts (Burson et al., 2016; Philippart et al., 2000). Additionally, water clarity decreased in large parts of the North Sea during the 20th century (Capuzzo et al., 2015). These abiotic changes affect primary productivity and community composition shifts throughout the trophic levels, with large implications for ecosystem functioning and fisheries production (Capuzzo et al., 2017; Burson et al., 2016). Over time, further changes are expected due to the planned energy transition and under the impact of climate change. Anticipated climate change effects include increasing temperatures, sea level rise, and ocean acidification. Already, the North Sea is warming more rapidly than most other seas (Philippart et al., 2011). These changing environmental conditions will have a big impact on marine biogeochemistry, phytoplankton community composition and primary productivity (Sarmiento et al., 2004; Behrenfeld et al., 2006; Marinov et al., 2010). Changes in phytoplankton community composition and primary productivity affect the entire ecosystem and global biogeochemical cycles (Montes-Hugo et al., 2009; Falkowski et al., 1998; Schiebel et al., 2017). Systematic and sufficient monitoring of these changes is of crucial importance to recognize threats, and, once identified as such, develop mitigation actions.

Although phytoplankton community composition and productivity can be highly variable on a spatial and temporal scale, governmental monitoring still consists mainly of low-resolution measurements (Baretta-Bekker et al., 2009; Kromkamp and van Engeland, 2010; Cloern et al., 2014; Rantajarvi et al., 1998). Currently, biological monitoring of phytoplankton in the Dutch North Sea is dictated by the requirements set by OSPAR and the EU Marine Strategy Framework Directive (MSFD 2008/56/EC). Samples are taken between March and October with a frequency of every two or four weeks. The phytoplankton analysis consists of HPLC analysis of Chl *a* concentration and microscopy counts of *Phaeocystis* cells and, at some stations, coccolithophore or toxic dinoflagellate cells. Sampling points were reduced from almost 70 in 1984 to less than 20 today, while strong seasonal patterns, high riverine input, and tidal forces make the Dutch North Sea a region with high spatiotemporal variability. Modern automated flow-through underway systems have the potential to be an effective addition to monitoring programs because they offer the opportunity to record the surface ocean with high spatial and temporal resolution. Such high-resolution methods are well established in physical oceanography but for biological parameters, the implementation has been lacking. This is mostly due to the complicated interpretation of biological parameters, resulting in high uncertainties in the current global estimates of net primary productivity (Silsbe et al., 2016). Underway measurements are not able to replace some more detailed low-resolution measurements, but their higher spatial and temporal resolutions provide the possibility to identify short-lived events, detect small-scale changes in phytoplankton dynamics, evaluate consequences of possible (spatial) undersampling, and act as an early warning system. Additionally, underway measurements acquire information on living organisms and samples unaffected by transport, storage or conservation. Two non-invasive, high-resolution methods with the potential to be implemented in phytoplankton monitoring programs are scanning flowcytometry (FCM) for information on phytoplankton abundance and community composition and Fast Repetition Rate fluorometry (FRRf) to give information on phytoplankton photophysiology. Scanning flowcytometry is a method for counting and pulse-shape recording of phytoplankton cells informative on size, fluorescence and scattering properties per algal cell. Based on these characteristics cluster analysis allows for division into groups of similar pigment characteristics and size classes (Thyssen et al., 2015; Rijkeboer, 2018). The FRRf uses active fluorescence to gain insight into phytoplankton photophysiology. This technique is an alternative to the traditional production-light curves (PE-curves) by estimating the photosynthetic electron transport rate (or gross photosynthesis) at increasing ambient light levels (Suggett et al., 2009a; Silsbe and Kromkamp, 2012). Electron transport rate per unit volume is estimated based on the fluorescence response to a series of single turnover light flashes that cumulatively close all photosystems (Kromkamp and Forster, 2003; Suggett et al., 2003). This single turnover technique allows

for the calculation of the effective absorption cross-section and, in combination with an instrument-specific calibration coefficient, the number of reaction centers per volume (Kolber et al, 1998; Kromkamp and Forster, 2003; Oxborough et al., 2012; Silsbe et al., 2015). Electron transport rate per volume can be used to estimate gross primary productivity (Kromkamp et al., 2008; Smyth et al., 2004; Suggett et al., 2009a). These two methods are supplementary because the interaction of phytoplankton with their environment is always a sum of the community composition and their physiology. For instance, if waters become more turbid, phytoplankton can acclimate by increasing their effective absorption cross section, but it could also lead to a shift in community composition toward species with higher light use efficiency (Moore et al., 2006). Thererfore, the combination of these two instruments allows for more in-depth analysis and understanding of ecosystem processes.

The aim of this study is to test two high-resolution methods, a pulse shape recording flowcytometer and an FRR fluorometer, on their potential to be developed into a novel phytoplankton monitoring method. The two instruments were deployed concurrently on four 4-day cruises in April, May, June, and August to meet a wide range of environmental conditions and phytoplankton community states. These measurements allow for quantification of temporal and mesoscale spatial patterns in phytoplankton abundance, photophysiology, and gross primary production. In this paper we provide an overview of the acquired results, use spectral cluster analysis to visualize spatial heterogeneity and we evaluate the potential of these methods to optimize current monitoring programs.

2 Methods

2.1 Study site and sampling

The Dutch North Sea is a shallow tidal shelf sea in the southern part of the North Sea. The main water flow is northward. Atlantic water enters the North Sea from the south via the Channel and from the northeast where it curves around Scotland. Both currents meet north of the Dutch coast forming the Frisian Front. For a detailed description on the North Sea physical oceanography, see Sündermann and Pohlman (2011). Along the Dutch coast, high river input from especially the Rhine River decreases the salinity and loads the coastal zone with high nutrient concentrations (Burson et al., 2016). Anthropogenic pressure is high in the Dutch North Sea resulting in a history of large shifts in nutrient concentrations and water clarity (Capuzzo et al., 2015; Burson et al., 2016). The monitoring of the Dutch North Sea is performed by the Dutch government (Rijkswaterstaat) in a monitoring program called MWTL (Monitoring Waterstaatkundige Toestand des Lands, freely translated as 'Monitoring of the status of the governmental waters of the country'). The locations of the sampling stations of the program are organized along transects (Fig. 1). The stations are sampled between March and October with a frequency of every two or four weeks, dependent on the transect.

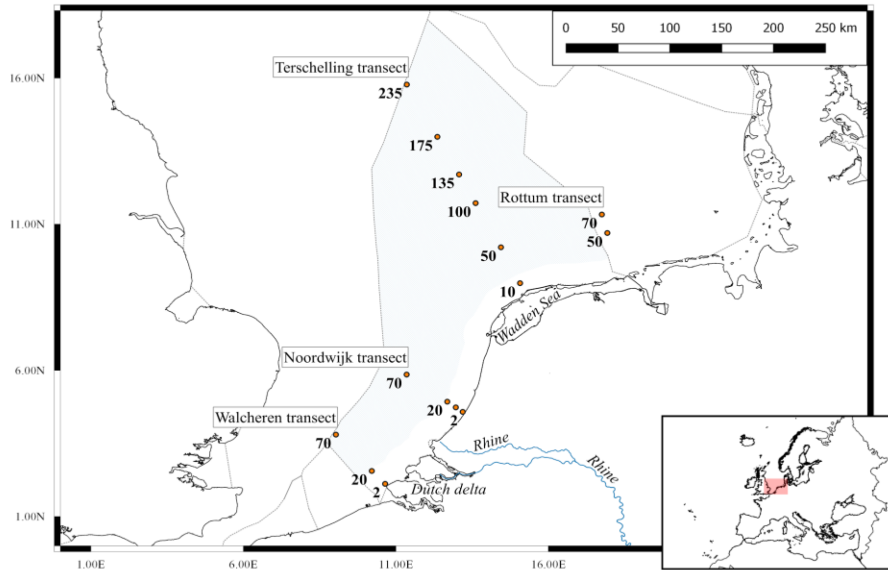

Figure 1: Sampling locations of the MWTL monitoring program referred to in this study. The stations are named according to the transect (Terschelling, Noordwijk and Walcheren), followed by the amount of kilometres from the coast (labels next to sampling points). The boundaries of the Exclusive Economic Zone (EEZ) are indicated by the grey dotted lines and the Dutch EEZ is coloured light blue. The locations of three major infows to the Dutch North Sea are named at the corresponding locations (Rhine river, Dutch Delta and the Wadden Sea). Insertion visualizes the location of the Dutch North Sea in a broader map of Europe.

In 2017, four 4-day sampling surveys (10-13 April, 15-18 May 12-15 June and 14-17 August), were conducted for the JERICO-NEXT project on board the RV *Zirfaea* during their regular monitoring cruises on the Dutch North Sea. To assess the heterogeneity of the Dutch North Sea and the benefits associated with high-resolution monitoring the four cruises were conducted in different months (April, May, June, and August), thereby aiming to cover different seasons and stages of the phytoplankton bloom (Baretta-Bekker et al., 2009).

The water inlet of the underway system was situated approximately 3.5 m below sea surface level. From the water inlet the sample water, with a flow rate of approximately 24 liters per minute, was split towards: 1) a flow-through -4H-JENA Ferrybox (-4H- JENA engineering GmbH, Germany) equipped with an FSI Excell® Thermosalinograph (Sea-Bird Scientific, USA) to measure temperature and salinity, and 2) a 230 cm^3 flow through sampling chamber (Cytobuoy BV, the Netherlands) where water was cleared from bubbles and sand (~ flow rate of 1 L per minute). The time from the water inlet to the sampling chamber was approximately 2 minutes. A FastOcean Fast Repetition Rate fluorometer (FRRf) with Act2-based laboratory flow-through system (Chelsea Technologies Group Ltd, UK) and a Cytosense scanning flowcytometer (Cytobuoy BV, the Netherlands) automatically sampled from the sampling chamber every 30 minutes. Since the average speed of the ship was 8 knots, the average spatial resolution of FCM and FRRf measurements was on average 7.5 kilometers. The Ferrybox sensors stored data every minute. During the cruises the high-resolution methods (FRRf, FCM, and Ferrybox) were combined with lower resolution methods, consisting of measurements at 13 to 19 stations. At these stations, surface samples were taken for nutrient and chlorophyll *a* analyses (see 2.2 chemical analyses) using a rosette sampler equipped with a CTD and Niskin bottles.

2.2 Chemical analyses

Samples for nutrient analyses were filtered over Whatmann GF/F filters and kept frozen (-18 °C) until analyses. The analyses of ammonium (NH_4^+), nitrite (NO_2^-), nitrate (NO_3^-), phosphate (PO_4) and silicate (Si) concentrations were conducted by the Rijkswaterstaat laboratory (RWS; the Netherlands) according to ISO 13395, 15681, 16264 using a San^{++} Analyzer (Skalar

Analytical B.V., the Netherlands). In the RWS internal protocol, nitrite+nitrate is measured by first reducing nitrate to nitrite using a cadmium/copper column and addition of ammoniumchloride as a buffer. Thereafter, sulphanilamide, α-naphthyl ethylenediamine dihydrochloride and phosphoric acid are added and the extinction at 540 nm compared to a $NaNO_2$ standard. For measurement of ammonium concentrations first EDTA was added to bind calcium and magnesium. Then, sodium salicylate, sodium nitroprusside and sodium hypochlorite were added and the extinction at 630 nm compared to a NH_4Cl standard. Phosphate was measured by adding molybdate reagent and ascorbic acid to the sample and led through an oilbath at 37 ± 2 °C. Followed by measuring the extinction at 880 nm and comparing to a standard. Silicate concentration was measured by subsequent addition of molybdate reagent, oxalic acid and ascorbic acid. The silicate concentration was then determined by measuring the extinction at 810 nm and compared to a silicate standard. The detection limits of the nutrient analyses were NO_3NO_2: 0.7 µM, Si: 0.36 µM and PO_4^{3-}: 0.03 µM.

Chlorophyll *a* concentration (hereafter Chl *a*) was determined by filtering over Whatmann GF/C filters and freezing the filter at -80 ºC. The Chl *a* was extracted in 20 ml 90% acetone and centrifuged for 15 minutes with glass pearls (1.00-1.05 mm) using a Bullet Blender Tissue homogenizer (Next Advance, Inc., Troy, USA) under cooling of solid CO_2. The extract was analyzed in duplicates using Ultra High Performance Liquid Chromatography (UHPLC). The calibration of the UHPLC system is performed every analysis day by making a 12-point standards calibration curve calculated using quadratic regression with weighting method 1/A to better distinguish smaller peaks (R^2>0.995). The injection volume was 20 µl unless the concentration was below the lowest standard, in which case a second injection of 40 µl was reanalyzed. The analysis was conducted by the MUMM laboratory (Belgium) using according to RWS analysis protocol A200. Quality control was performed by the RWS laboratory (The Netherlands).

2.3 High frequency methods

2.3.1 Variable fluorescence

Variable fluorescence was measured with a FastOcean Fast Repetition Rate fluorometer (FRRf) and Act2-based laboratory system (Chelsea Technologies Group Ltd, UK). The temperature was controlled by connecting a Lauda ecoline cooler (LAUDA-Brinkmann, LP., USA) to the water jacket of the Act2 system.

The acquisition protocol consisted of 100 excitation flashes with a flash pitch of 2 µs and 40 relaxation flashes with a flash pitch of 60 µs. Excitation flashes were performed with the blue LED (450 nm) and strength of the LEDs was automatically adjusted to the phytoplankton concentration by the manufacturer' FAstPro software. A loop of simultaneous blue and green flashes (450 nm+530nm) was performed after the acquisition loop of only blue LEDs in case the blue LEDs were not able to reach saturation (for instance with high cyanobacteria concentrations), but as this was not the case, only the parameters measured by blue LEDs were used for further calculation. The sequence was repeated 20 times with a sequence interval of 100 ms. The sample was refreshed before each Fluorescent Light Curve (FLC) by flushing for 60 seconds and kept well-mixed by "flushing" for 200 ms between acquisition loops.

The FLC protocol consisted of 14 light steps of 100 s, of which the light intensity was automatically adjusted to get the optimal FLC shape based on the previous light curve. A pre-illumination step (55 seconds on 12 µmol photons m^{-2} s^{-1}) was included before the FLC to low light acclimate the phytoplankton and to relax Non-Photochemical Quenching (NPQ) of diatoms and other chlorophyll *a-c* algae as they stay in the light activated state in the dark (Goss et al., 2006). After each light step, measurements were made in the dark for 18s to retain a value for F_0' (minimal fluorescence in light acclimated state). The data were corrected for the background fluorescence by taking sample blanks multiple times per day by filtration over a 0.45 µm filter and subtracting the last determined background fluorescence from the sample fluorescence.

An overview of the derived photosynthetic parameters can be found in Table 1. To derive values for the maximum photosynthetic electron transport rate (P_{max}), minimum saturating irradiance (E_k) and the light utilisation efficiency (α) the relative electron transport rate (rETR) of the samples was fitted to the exponential model of (Webb et al. 1974), after normalizing the data to the irradiance as described by (Silsbe and Kromkamp, 2012):

5

$$F_q'/F_m' = \frac{P_{max}\left(1-\exp\left(\frac{-E}{E_k}\right)\right)}{E} \quad (1)$$

where E is the irradiance in μmol photons m^{-2} s^{-1}, F_q'/F_m' the effective quantum efficiency of photosystem II (PSII), α is the initial slope of the rETR vs irradiance curve and E_k is the light saturation parameter (in μmol photons m^{-2} s^{-1}). The relative maximum rate of photosynthetic electron transport (P_{max}) was calculated as:

10

$$P_{max} = E_k \times \alpha \quad (2)$$

The PSII flux in μmol electrons m^{-3} h^{-1} was calculated as the product of the effective PSII efficiency (F_q'/F_m'), the optical absorption cross section of the light harvesting pigments of PSII (a_{LHII}) and the irradiance (E):

15

$$JV_{PII}(\text{ in } \mu mol\ electrons\ (PSII\ m^{-3})\ h^{-1}) = F_q'/F_m' * a_{LHII} * E \quad (3)$$

where

$$F_q'/F_m' = \frac{F_m' - F'}{F_m'} \quad (4)$$

and

$$a_{LHII}\ (in\ m^{-1}) = \frac{F_0 * F_m}{F_m - F_0} * K_a \quad (5)$$

20

Table 1: The derived photosynthetic parameters used in the text (see Oxborough et al. (2012) and Silsbe et al. (2015) for more information). Variables used in equation 1-8 are not included but discussed in the text.

	Description	**unit**
Parameters derived from fluorescence induction curve		
F_0	Minimum fluorescence, measured at zeroth flashlet of an FRRf single turnover measurement when all PSII reaction centers (RCII) are open. Estimate for chlorophyll *a* concentration.	Dimensionless
F_m	Maximum fluorescence, reached at nth flashlet of an FRRf single turnover measurement when all PSII reaction centers are closed.	Dimensionless
1/τ	Rate of re-opening of a closed RCII	ms^{-1}
σ_{PSII}	Effective absorption cross section of PSII photochemistry	nm^2 $PSII^{-1}$
Parameters calculated from parameters derived from fluorescence induction curve		
JV_{PII}	PSII charge separation rate per unit volume (see eq. [3])	μmol electrons m^{-3} h^{-1}
F_v/F_m	Quantum efficiency of PSII under dark conditions (see eq. [4])	Dimensionless
a_{LHII}	Absorption coefficient of PSII light harvesting (see eq. [5])	m^{-1}
[RCII]	Functional PSII reaction centers per volume (see eq. [6])	nmol RCII m^{-3}
Parameters derived from Fluorescence light curve (FLC)		
α_{PSII}	Initial slope of the FLC, an estimate of affinity for light	μmol electrons (μmol photons) $^{-1}$
E_k	Minimum saturating irradiance of fluorescence light curve	μmol photons m^{-2} s^{-1}
P_{max}	Maximum photosynthetic electron transport rate	μmol electrons m^{-2} s^{-1}
Parameters calculated from parameters derived from fluorescence light curve and irradiance		
Surface GPP	Surface Gross Primary Productivity (see eq. [3]) calculated based on the FLC-parameters and incoming irradiance.	μg C L^{-1} h^{-1}

25

K_a (m^{-1}) is an instrument specific factor necessary for obtaining absolutes rate of photosynthetic transport (see Oxborough et al. (2012) and Silsbe et al. (2015) for more information). The amount of reaction centres of PSII per cubic metre ([RCII]) was calculated as

$$[RCII]\ (in\ nmol\ m^{-3}) = K_a * \frac{F_0}{\sigma_{PSII}} \quad (6)$$

for more information on the calculation of [RCII] and a_{LHII} see Oxborough et al. (2012) and Silsbe et al. (2015).
Q_A reoxidation or rate of re-opening of a closed RCII was calculated as 1 divided by the time constant of re-opening of a closed RCII with an empty Q_B site (τ_{ES}) in ms^{-1}.

Standardized daily anomalies (Z-scores) were calculated for the photophysiological parameters as:

$$Z - score = \frac{x - daily\ mean(x_0 \ldots x_{24})}{Daily\ standard\ deviation(x_0 \ldots x_{24})} \quad (7)$$

Partial days were excluded because this could potentially offset the daily mean and standard deviation.

Gross Primary Productivity (GPP) was estimated by fitting JV_{PII} in µmol photons m^{-3} h^{-1} to equation 1 (the exponential model of Webb et al., 1974) to derive a volumetric P_{max} and α. GPP in µg C L^{-1} h^{-1} was then calculated using equation 1 and incident surface irradiance. To avoid effects of changing incident surface irradiance ($E_{surface}$) on the spatial pattern and to be able to compare GPP between regions we used monthly average surface irradiances ($E_{surface}$) in our calculations of primary productivity. From 2010-2016 irradiance (400-700 nm) was measured at the roof of the NIOZ building in Yerseke using a LI-190 quantum PAR sensor and hourly averages stored using a LI1000 datalogger. $E_{surface}$ was then calculated by averaging all irradiance data from the years 2010-2016 for the respective month. The primary productivity in electrons units was converted to carbon units by assuming 6 moles of electrons were required to fix one mole of carbon, based on a study in the adjacent Oosterschelde and Westerschelde estuaries (Kromkamp et al., in prep.).

2.3.2 CytoSense scanning flowcytometry

Single cell measurements of the phytoplankton community were conducted using a bench-top scanning flowcytometer (Cytobuoy BV, the Netherlands) equipped with two lasers (488 nm and 552nm; 60mW each). Both laser beams were ca. 5 µm high and 300 µm wide and focussed on the same spot in the middle of the flow-through chamber. The speed of the particles was ca. 2.2 m s^{-1}. The system contained 3 fluorescence detector channels separating fluoresced wavelengths of 550-600 nm (FLY; Phycoerythrin), 600-650 nm (FLO; Phycocyanin) and above 650 nm (FLR; chlorophyll *a*). Additionally, the Forward Light Scatter (FWS) and Sideward Light Scatter (SWS) of all particles were measured. The FCM was equipped with a double set of detectors (PMT's) for each of the three fluorescence channels to increase the dynamic range (Rutten, 2015). Per cell, the pulse shape of the parameters (FWS, SWS, FLR, FLO, and FLY) plus their affiliates (length, total and maximum values) were recorded and saved. The instrument was checked daily for drift using 3 µm Cyto-Cal™ 488 nm alignments beads (Thermo Fisher Scientific Inc., USA). Additionally, the FCM was equipped with an Image-in-flow camera to take pictures of the nano- and micro-phytoplankton. This allows for linking pulse shape recordings to microscopy results and thereby identification of represented phytoplankton groups in respective clusters.

Phytoplankton cells were clustered based on the pulse shape recording of the individually scanned phytoplankton. In this paper, we discriminate the phytoplankton groups based on their size (pico, nano, and micro) and Orange/Red fluorescence ratio (hereafter O/R ratio; Table 2). The chosen cluster criteria were based on expert judgment (SeaDataNet, 2018) and corresponding to other studies (Sieburth et al., 1978; Vaulot et al., 2008). The clustering was done using the software Easyclus 1.26 (ThomasRuttenProjects, The

Table 2: The phytoplankton groups distinguished in the current study.

Name	Cluster criteria		Main corresponding taxonomic group(s)
	Length FWS	O/R-ratio	
Pico-Red	<4 µm*	<1	Pico-eukaryotes
Pico-Synecho	<4 µm*	>1	Synechococcus
Nano-Crypto	4-20 µm	>1	Cryptophycea
Nano-Red	4-20 µm	<1	Diatoms,Haptophytes, Dinoflagelates
Micro-Red	>20 µm	<1	Diatoms,Haptophytes, Dinoflagelates

*In june <6 µm

5 Netherlands) according to these criteria. Noise, air bubbles and other potential outliers were removed. The acceleration of the particles in the sheath fluid positions the cells along their long axis, which allows for size estimation based on the FWS pulse shape. A linear relation was found between Length FWS and measured length of diverse phytoplankton species (Length FWS = 0.92*Measured length – 1.57; R^2=0.98; Rijkeboer, 2018). Size estimation is limited by the width of the laser beam (5 µm) so estimations of cell sizes < 5 µm is not possible based on the FWS.

10

2.4 Data analysis

Outliers of the complete dataset were removed after visual inspection of pairplots made with the pairplot function of the HighstatLib.V4 script (Zuur et al., 2009). For the FRRf data, quality control of the FLC fits was done based on the quality ratio of the induction curve fit per FLC light step and the r^2 of the FLC fit. The quality ratio of the induction curve fit was calculated as the
15 ratio of Fv or Fv' to the standard error (SE) of the linear regression of the saturation phase. FLC fits with an r^2 < 0.75, or with over 30% of the data points with a quality ratio below 6, were visually inspected and removed based on expert judgment. This led to the removal of 1% to 7% of the FLC fits per month. Unsatisfactory fits occurred when the auto-LED settings misadjusted the maximum irradiance or when fluorescence was too low to retrieve a reliable fluorescence signal. Especially at low biomass FLCs became noisy, therefore a minimum fluorescence signal was set for calculations of photosynthetic parameters. Below this blank corrected
20 instrument-specific fluorescence signal F_q'/F_m' became noisy and often reached above the biologically unlikely limit of 0.65 (Kolber and Falkowski, 1993). The datasets of the high-resolution measurements (FRRf, FCM, and Ferrybox) were linked using corresponding timestamps. When multiple measurements were performed within one FLC, the average was used. To test whether environmental conditions (as present in the different months) had a significant effect on fluorescence as a predictor for Chl *a* concentration, an ANCOVA was performed with the month as a factorial predictor. To find regions with similar phytoplankton
25 communities, data were spectrally clustered using the uHMM R package (Poisson-caillault and Ternynck, 2016) in the statistical software R (version 3.4.1, R Core Team, 2017). The package default settings normalize data before clustering and automatically find the number of clusters based on spectral classification and the geometry of the data. This new methodology is more robust than the classical hierarchical and k-means technics (Rousseeuw et al., 2015). Phytoplankton parameters were first tested for collinearity and predictors with a variance inflation factor (VIF) over 6 were removed (Zuur et al., 2009; see supplementary material for
30 pairplots). This left for the cluster analysis FCM-parameters Pico-red, Nano-red, Micro-red, and *Synechococcus* and the FRRf-parameters σ_{PSII}, F_v/F_m, a_{LHII}, $1/\tau$, E_k. Datapoints were then per cluster labeled and plotted on a map to visually identify regions. Principal Component Analyses (PCA) were performed to find which variables contributed most to the cluster results. The PCA's were based on correlation matrixes with scaled parameters to correct for unequal variances and was carried out with the prcomp() function in R (version 3.4.1, R Core Team, 2017). The PCA visualization was done using the supplemental R package factoextra
35 (Kassambra and Mundt, 2017). Maps were made using QGIS v. 2.14.2 and other figures were made with ggplot2 in R (Wickham, 2009).

3 Results

3.1 Abiotic conditions

Environmental conditions in the Dutch North Sea were spatially heterogeneous and differed strongly between months. Sea surface temperature increased from 9.5 ± 1.0 ºC in April to 19.0 ± 0.6 ºC in August (supplementary table S1). Differences in salinity between cruises were small with the highest monthly mean salinity in April (34.1 ± 1.8). Spatial variability of salinity was higher with river influx decreasing the salinity down to 26 in the coastal zone. The monthly average of turbidity was higher in April (2.3 ± 3.0 NTU) in comparison to other months. This was also reflected in the K_d values, which were highest in April (0.39 ± 0.28 m^{-1}; supplementary table S1). It needs to be noted that monthly averages are not fully comparable, because of differences in sampling route and stations (Fig. 3). Dissolved Inorganic Nitrogen (DIN; Nitrate+Nitrite+Ammonium) and silicate (Si) concentrations showed spatial variability and varied per cruise (supplementary table S2). Spatially, two trends were distinguishable: a coastal-offshore gradient and a longitudinal gradient. Per cruise the strength and position of these spatial gradients changed. The coastal to offshore gradient moved shoreward from April to August and the southern stations were depleted earlier in the year in comparison to the more northerly stations. In April DIN and Si concentrations were on average higher and only potentially limiting (Si<1.8 µmol L^{-1}, DIN<2 µmol L^{-1}; Peeters and Peperzak et al. (1990) and references therein) in the most Southerly part of the Dutch North Sea (Walcheren transect) and at offshore stations (>70 km offshore west of the Netherlands, >135 km North of the Netherlands). In later months, DIN and Si limitations gradually moved towards the coastal zone. Stations closest to freshwater influx (Noordwijk 2 and 10) became DIN and Si-limited later in the year (supplementary table S2). The increased DIN concentration at the transect close to the Rhine outflow was absent seventy kilometers offshore (Noordwijk 70), suggesting that the Rhine water remained close to the coast. Phosphate concentrations were low and possibly limiting throughout the Dutch North Sea (ortho-phosphate PO_4^{3-}<0.5 µmol L^{-1}; Peeters and Peperzak et al, 1990). With exceptions in April north of Terschelling between 50 and 100 km offshore and in May at Noordwijk 2, a region with the high freshwater influx. In June and August, phosphate concentrations recovered in the Southern part of the Dutch North Sea reaching up to 0.6 µM (supplementary table S2).

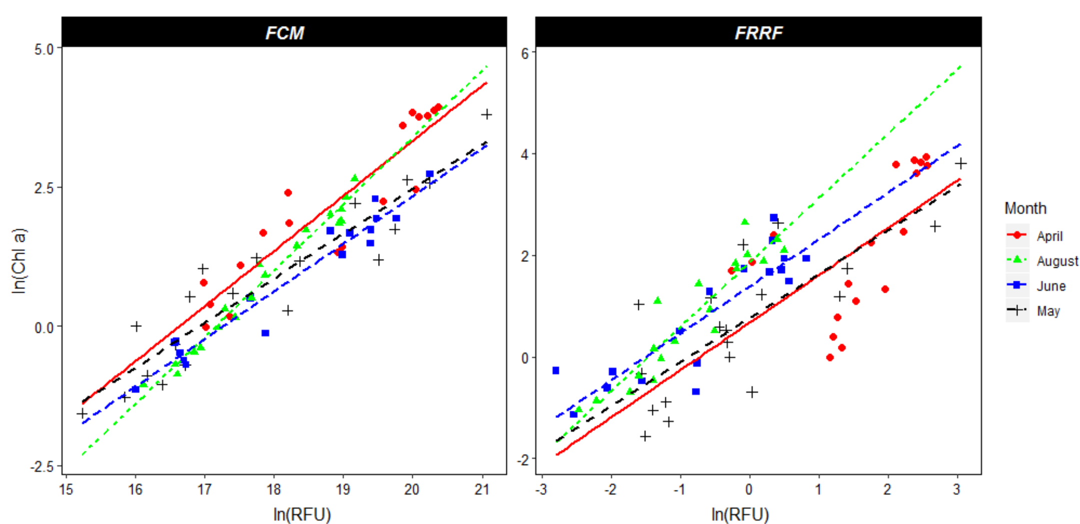

Figure 2: linear regression of the natural logarithms of Chl *a* concentration in µg L^{-1} as determined by HPLC (y-axis) and on the x-axis the natural logarithm of; FCM-derived total red fluorescence (in relative fluorensence units (RFU), left panel) and FRRf-derived minimum fluorescence (F_0 in RFU, right panel). Both FCM red fluorescence (p<0.01, adjusted R^2=0.90) and the FRRF F_0 (p<0.01, adjusted R2=0.66) are significant predictors for Chl *a* concentrations. The months (April, May, June and August) were a significant predictor of Chl *a* concentration for both the FRRf (p<0.05) and the FCM (p<0.01). The interaction between the x and y axis was only significant for the FCM data (p<0.05).

3.2 Phytoplankton abundance and fluorescence

Before the ANCOVA analysis, natural logarithm transformations were required to correct for inhomogeneity of the residuals and unequal variances between months. Both the FRRf F_0 ($p<0.01$, adjusted $R^2=0.66$) and FCM total red fluorescence ($p<0.01$, adjusted $R^2=0.90$) provided significant predictors of HPLC-derived Chl *a* concentration (Fig. 2). The ANCOVA with the FRRf-derived F_0 as Chl *a* predictor revealed that the slope did not differ per month, but the intercept did ($p<0.01$). The ANCOVA with the FCM-derived TFLR as Chl *a* predictor resulted not only in a significant difference of the Chl *a* concentration per month ($p<0.01$) but also in a significantly different slope ($p<0.05$), suggesting that other predictors that differ per month were influencing the fluorescence per Chl *a* molecule (Fig. 2).

3.3 Phytoplankton community composition

In April the northern part of the Dutch North Sea was numerically dominated by picoplankton whereas the southern part and the north coastal area of the Dutch EEZ were numerically dominated by nanophytoplankton. The taxa with high phycoerythrin content (*Synechococcus* and Cryptophycea) made up only a small proportion of the total phytoplankton community in April (generally less than 10%) and were most abundant in the northern part of the Dutch North Sea (Fig. 3e). Microphytoplankton represented always less than 3% of the total community. Highest microphytoplankton abundance was found close to the Dutch Delta and along the Noordwijk transect. The spatial patterns of the phytoplankton community in May were smaller in comparison to April (Fig. 3, second column). Picophytoplankton abundance was highest offshore (60-80%), whereas the highest percentage of nanophytoplankton was observed north of Terschelling 100 and in the coastal zone (Fig. 3f). Between May and June the community composition shifted and phytoplankton cell numbers increased. Both groups of picophytoplankton (*Synechococcus* and Pico-red) increase in relative abundance between May and June, while the nano-phytoplankton shows a strong decrease (Fig. 3). The highest abundance of pico-phytoplankton was observed offshore. The microphytoplankton was the largest contributor to red fluorescence in the coastal region, although this group does not increase in relative abundance in comparison to May (Fig. 3). In August the pico-phytoplankton was dominating the phytoplankton communities with an average contribution to total cell numbers of over 80% and only slightly lower values were observed (but still > 70%) along the southern Dutch coast, where the abundance of nano-phytoplankton was higher. Micro-phytoplankton was hardly observed, although their high per cell red fluorescence, they contributed to up to half of the total red fluorescence in coastal regions.

3.4 Photophysiology

In April, the photophysiology of the phytoplankton communities in the Dutch North Sea showed low variability. The F_v/F_m values stayed above 0.5 in northern regions and above 0.4 in southern regions (Fig. 4a). The σ_{PSII} stayed in a narrow range between 2.5-4 nm^2 $PSII^{-1}$ (Fig. 4e). The E_k in April showed more variability in comparison to the F_v/F_m and σ_{PSII}. In the coastal zone, the E_k was lower off the coast from Walcheren and higher off the coast from Noordwijk. In offshore regions, no clear spatial patterns were present (Fig. 4i). In May photophysiological parameters of the phytoplankton communities in the Dutch North Sea were strongly heterogeneous with only smaller scale spatial patterns (Fig. 4b,f,j). F_v/F_m was in general lower in May (0.1-0.5) than in April (>0.4) across most of the Dutch EEZ (Fig. 4b). In May the σ_{PSII} was high (average 5.9 nm^2 $PSII^{-1}$) across the Dutch North Sea, except near the coast of Noordwijk (Fig. 4f). In the same region, the E_k was high (> 450 µmol photons m^{-2} s^{-1}), but this concurrent signal (high E_k, low σ_{PSII}) did not occur in other regions of the Dutch North Sea. The E_k across the Dutch North Sea in May was heterogeneous without large-scale spatial patterns. In June the spatial patterns in the photophysiology of the phytoplankton in the Dutch North Sea were less heterogeneous and larger mesoscale spatial patterns could be identified. The F_v/F_m values recovered in comparison to May to above 0.4 in the coastal zone, but not in offshore regions in the Southern North Sea. The F_v/F_m of the southern offshore

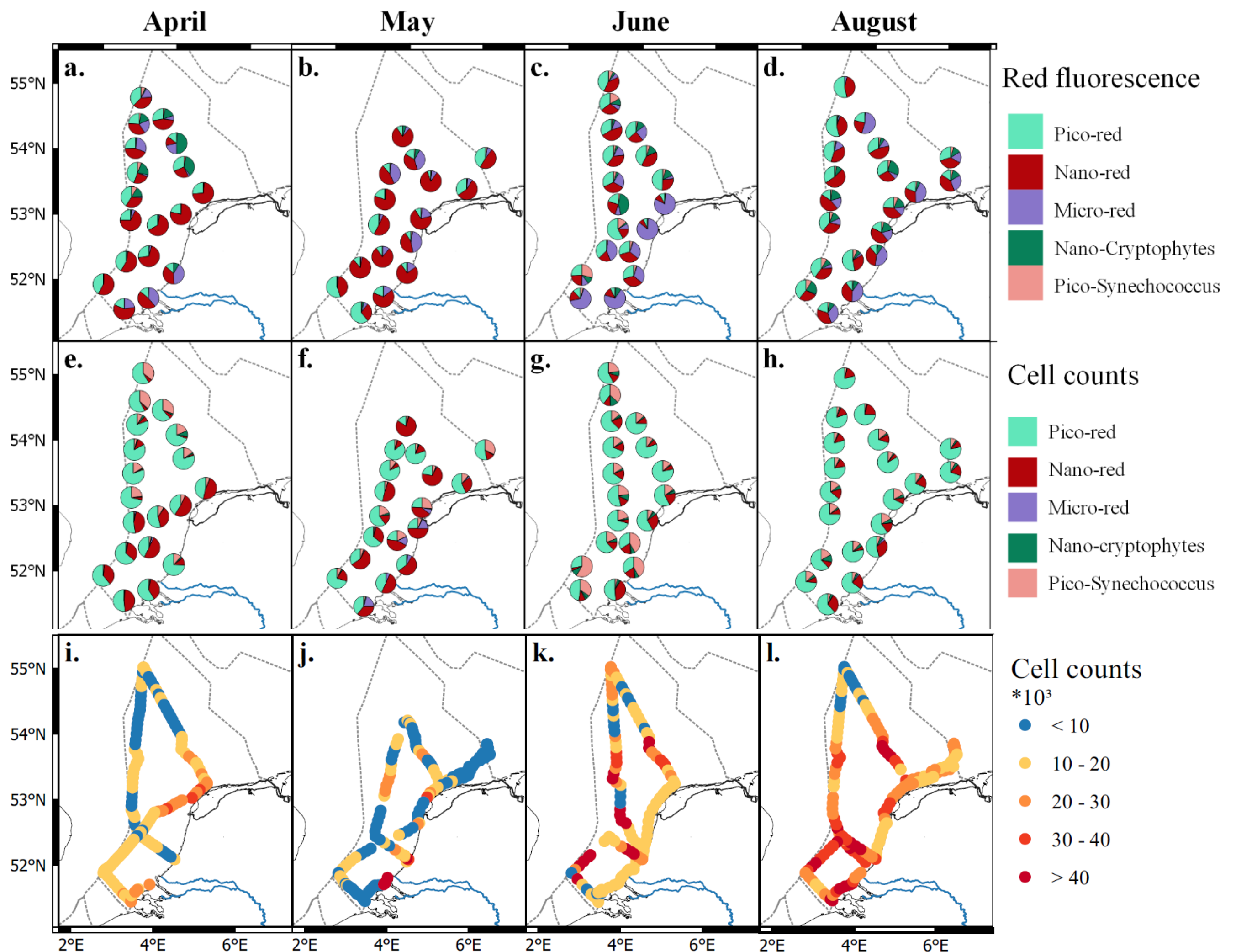

Figure 3: Relative phytoplankton community composition using FCM-derived total red fluorescence (first row; a-d) and cell numbers (second row, e-h) in April, May, June and August (from left to right). The groups are clustered according to table 2.

phytoplankton, between Walcheren 70 and Noordwijk 70 (Fig. 1), remained low (<0.2; Fig. 4c). The σ_{PSII} was lower in comparison to May across the Dutch North Sea, apart from the southern offshore region (Fig. 4g). In a small region around Noordwijk 70, the phytoplankton community had a particularly low σ_{PSII} (<2.5 nm^2 PSII^{-1}) which did not present itself in anomalies in the other photophysiological parameters. The E_k in June was low in the Northern coastal zone and higher in offshore regions (Fig. 4k). In August the F_v/F_m recovered across the Dutch North Sea (Fig. 4d). The σ_{PSII} was high in the northern offshore region, and comparable to June in the rest of the Dutch North Sea (Fig. 4h). In August the regions of the Noordwijk coast and the of the Wadden Island coast were sampled twice, on two different times of the day. This repeated measurement resulted in a higher E_k, suggesting diurnal variability. To further investigate daily patterns standardized daily anomalies (z-scores) were calculated. These show a clear diurnal trend in photosynthetic activity (Fig. 5). The F_v/F_m was lowest during the middle of the day, while Ek, $\sigma_{PSII,}$ and $1/\tau$ peaked during the middle of the day. As E_k was strongly correlated to P_{max} (Fig. S2); a clear diurnal pattern was also present in the photosynthetic electron transport rate.

Figure 4: Maps of the photophysiological parameters Fv/Fm (a-d), σ_{PSII} (e-h; in nm^2 PSII^{-1}) and E_k (i-l; in µmol photons m^{-2} s^{-1}) per month (from left to right: April, May, June and August). For more details on the location see Fig. 1.

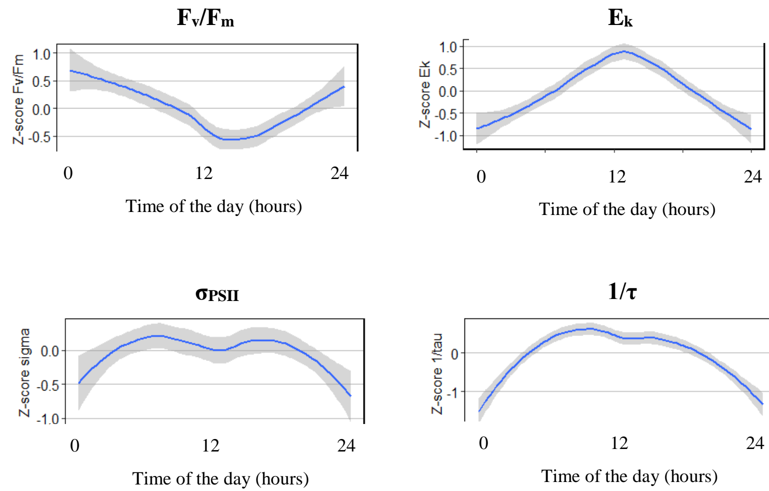

Figure 5: Standardized daily anomalies (z-scores) of F_v/F_m, E_k, σ_{PSII} and $1/\tau$ showing the diurnal trends in photophysiological data. On the x-axis the time of the day and on the y-axis the z-score.

3.5 Gross primary productivity

Gross primary productivity ranged from 0.35 µg C L^{-1} h^{-1} in June to 602 µg C L^{-1} h^{-1} in the coastal zone in May (Fig. 6). The average GPP was highest in April and lowest in August. Monthly averages ranged from 116 ± 59 µg C L^{-1} h^{-1} in April and 8.7 ± 8.3 µg C L^{-1} h^{-1} in August, although these averages are not completely comparable due to different ship routes per month (Fig. 6). In April,
5 spatial heterogeneity in GPP was low. Highest rates in April were measured offshore (> 250 µg C L^{-1} h^{-1}) and in the coastal regions close to the Wadden Islands (Terschelling 10 in Fig. 1). In May, the GPP was heterogeneous without a clear spatial pattern. Most production rates stayed below 30 µg C L^{-1} h^{-1}, with local GPP peak rates over 600 µg C L^{-1} h^{-1} in the southern coastal zone. In June, the GPP was on average lower than in May and showed more large-scale spatial patterning. Highest values in June were observed (30-40 µg C L^{-1} h^{-1}) northwest of Noordwijk. In August, GPP was low throughout the Dutch North Sea with the majority of
10 productivity rates staying below 10 µg C L^{-1} h^{-1}. In the southern coastal zone, slightly higher rates were found, reaching up to 50 µg C L^{-1} h^{-1}.

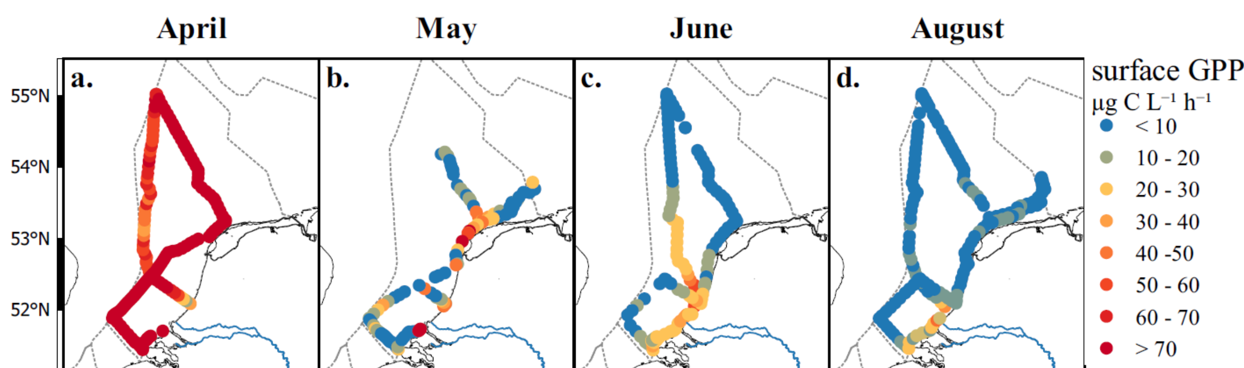

Figure 6: Gross primary productivity of the surface (a-d; in µg C L^{-1} h^{1}) per month (from left to right: April, May, June and August). Colors represent rates, where blue is low and red is high (see legend).

15 **3.5 Spatial clustering**

Strong collinearity between measured parameters was present. For spatial clustering these were removed based on the variable inflation factor (VIF>6; see supplementary material for pairplots), which resulted in the removal of the photophysiological parameters P_{max}, α, a_{LHII}, n_{PSII}, the FCM-parameter of the total red fluorescence and the GPP. From the five defined phytoplankton groups (Table 2), the nano-crypto group was not used in the clustering because of collinearity (VIF>6). The remaining variables
20 were the abundance of the remaining four FCM-defined phytoplankton groups (Pico-Red, Pico-Synecho, Nano-Red, and Micro-Red), the total O/R ratio and five photophysiological parameters (F_v/F_m, σ_{PSII}, 1/τ, [RCII], and E_k). For an overview of the collinearity between variables, see the pairplots in the supplementary material.

Spectral cluster analysis resulted in the identification of two to four clusters in each cruise. Most of these clusters were spatially
25 separated and therefore, can be considered as regions with distinct phytoplankton communities (Fig. 7). In April, the clustering resulted in three clusters with a clear spatial pattern. In the PCA, the variables that contributed most to the first principal component were all biomass related; [RCII] and a_{LHII}, related to the photosynthetic capacity per reaction center and per volume, and the abundance of the Nano-red group. The second principal component has photosynthetic parameters as two main contributors

30

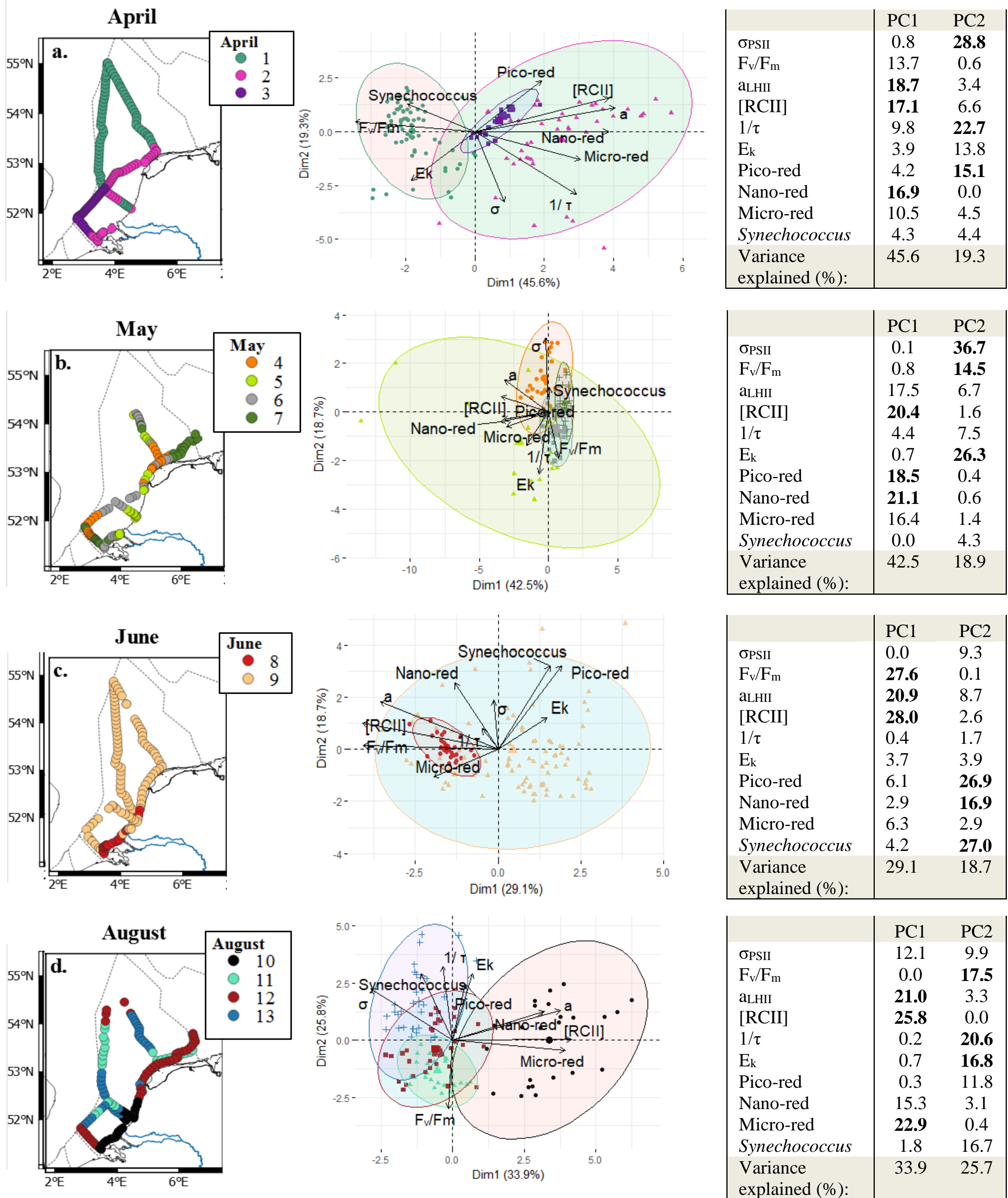

	PC1	PC2
σ_{PSII}	0.8	**28.8**
F_v/F_m	13.7	0.6
a_{LHII}	**18.7**	3.4
[RCII]	**17.1**	6.6
$1/\tau$	9.8	**22.7**
E_k	3.9	13.8
Pico-red	4.2	**15.1**
Nano-red	**16.9**	0.0
Micro-red	10.5	4.5
Synechococcus	4.3	4.4
Variance explained (%):	45.6	19.3

	PC1	PC2
σ_{PSII}	0.1	**36.7**
F_v/F_m	0.8	**14.5**
a_{LHII}	17.5	6.7
[RCII]	**20.4**	1.6
$1/\tau$	4.4	7.5
E_k	0.7	**26.3**
Pico-red	**18.5**	0.4
Nano-red	**21.1**	0.6
Micro-red	16.4	1.4
Synechococcus	0.0	4.3
Variance explained (%):	42.5	18.9

	PC1	PC2
σ_{PSII}	0.0	9.3
F_v/F_m	**27.6**	0.1
a_{LHII}	**20.9**	8.7
[RCII]	**28.0**	2.6
$1/\tau$	0.4	1.7
E_k	3.7	3.9
Pico-red	6.1	**26.9**
Nano-red	2.9	**16.9**
Micro-red	6.3	2.9
Synechococcus	4.2	**27.0**
Variance explained (%):	29.1	18.7

	PC1	PC2
σ_{PSII}	12.1	9.9
F_v/F_m	0.0	**17.5**
a_{LHII}	**21.0**	3.3
[RCII]	**25.8**	0.0
$1/\tau$	0.2	**20.6**
E_k	0.7	**16.8**
Pico-red	0.3	11.8
Nano-red	15.3	3.1
Micro-red	**22.9**	0.4
Synechococcus	1.8	16.7
Variance explained (%):	33.9	25.7

Figure 7: Overview of the spectral cluster analysis based on the non-collinear phytoplankton parameters (FCM: Pico-red, Nano-red, Micro-red, *Synechococcus*. FRRf: σ_{PSII}, F_v/F_m, a_{LHII}, $1/\tau$, E_k) separated per month (top to bottom: April, May, June and August). With on the left clusters visualized on maps and in the middle the bi-plots of the PCA of the data with confidence ellipses per cluster (confidence 95%). In all graphics clusters are visualized by different colors as shown in the legend inset. Of the confidence ellipses the border lines (and not the fill) correspond to the clusters. In the bi-plot overlapping confidence ellipses suggest a high similarity between groups while the size of the ellipse is a measure of variability within the group. On the right the table of the PCA analysis with contribution in % of the different variables, in bold the three variables that contribute most to the principal component.

(σ_{PSII} and $1/\tau$; 51.5%). Cluster one covered most of the Northern part of the Dutch North Sea, and a small part of the Noordwijk transect to the coast. The bi-plot of the PCA showed that the first cluster was negatively correlated to the main contributors of PC1 ([RCII] and a_{LHII}; Fig. 7), so this region consisted of a phytoplankton community with lower photosynthetic capacity per liter. The

coastal region was separated into two clusters, 2 and 3, with overlapping confidences ellipses (Fig. 7). The confidence interval of cluster 2 is larger than cluster 3, suggesting that the phytoplankton community in cluster 2 was more heterogeneous. Both clusters are positively correlated to the main contributors to PC1 ([RCII] and a_{LHII}), meaning these clusters consists of a community with higher photosynthetic capacity per volume. In May, the cluster analysis resulted in four different clusters, but without a well-defined spatial pattern. The PCA biplots showed that the confidence interval of cluster 5 overlaps most of the other clusters, indicating that this cluster has weak support. E_k was negatively correlated with cluster 4 and σ_{PSII}, suggesting that cluster 4 contained low light acclimated algae. In contrast, in June only two clusters with a distinct separation between coastal and offshore phytoplankton communities were found. The PCA showed that the offshore phytoplankton community was consisting of a diverse phytoplankton community while the coastal phytoplankton community with high F_v/F_m, a_{LHII} and [RCII]. In August not all clusters were spatially separated (Fig. 7). Different clusters were appointed to the same region visited within a two-day time span twice; in the north-eastern coastal region and at the transect of Noordwijk. Both times, cluster 11 is one of the overlapping spatial clusters. Cluster 11 corresponds to only night-time sampling periods and was defined by low E_k and low $1/\tau$, indicative of a low light acclimated phytoplankton community. This suggests that cluster 11 was a temporal cluster instead of a spatial cluster. To test this we repeated the analysis for the month of August but only including the measurements performed within an 8-hour timeframe around noon (12:00±4h; see supplementary material Fig. S4). In this timeframe, the southern coastal zone was distinct from the rest of the Dutch North Sea and corresponded to cluster 10 in the analysis of the complete dataset (Fig. 7d), so this cluster was defined by spatial variability. Cluster 12 and 13 were grouped together in the 12±4h timeframe as cluster 1. Cluster 11 was not recognized as a cluster within the 12±4h timeframe, so seemed indeed controlled by temporal rather than spatial variability.

4 Discussion

The objective of this study was to evaluate the added value of FRR fluorometry and flowcytometry for monitoring purposes. During four cruises spread over 5 months, a wide variety of environmental conditions and phytoplankton community states were sampled. Here, this data is used to evaluate the potential of this approach to be developed as a novel method to improve existing monitoring (OSPAR, MSFD).

Biomass is an important parameter to understand the role of phytoplankton in the ecosystem and biogeochemical cycles. Its direct measurement using high-resolution methods is challenging. Chlorophyll *a* concentration is often used as an estimate for biomass, although the Carbon:Chl *a* ratio is dependent on abiotic conditions and species-specific phenotypic plasticity and chlorophyll *a* is therefore not directly related to biomass (Flynn, 1991, 2005; Geider et al., 1997; Alvarez-Fernandez and Riegman, 2014; Halsey and Jones, 2015). In this study, chlorophyll concentrations are estimated by red fluorescence, which results in a good fit for both the FRRf (adjusted R^2=0.66) and the FCM (adjusted R^2=0.90). The impact of abiotic conditions on fluorescence as a predictor for chlorophyll *a* content was tested by comparing the relationship in the different months. Only the flowcytometer data were significantly affected by environmental conditions. The different environmental conditions per month did not affect the regression line of the FRRF data. Since the two instruments differ in optics as well as measurement set-up (measurements per cell vs bulk), differences are not surprising. The different measurement set-up, with the flowcytometer measuring the fluorescence per particle, while the FRRf does a measurement of the bulk sample, might blur the effect of environmental conditions. In a bulk measurement, other particles in solution scatter the excitation and emission photons, plus the emitted fluorescence of the phytoplankton is subject to reabsorption, especially at higher biomass densities. Yet, the difference most affected by environmental conditions is the

fluorescent state of the photosystems. The strong laser of the flowcytometer can only measure the maximum fluorescence (F_m), which is a parameter more prone to quenching than the minimum fluorescence measured by the FRRf. The lower sensitivity to environmental conditions implies that the FRRf is better suited to estimate chlorophyll *a* concentration in comparison to the FCM. Other studies that estimate chlorophyll *a* concentrations with FCM and fluorimeter also find better fits using the bulk measurements by a fluorimeter in comparison to the per cell flowcytometric measurements (Thyssen et al., 2015; Marrec et al., 2018). An alternative to the controversial use of chlorophyll *a* as an estimate for biomass is the derivation of biomass or biovolume from cell counts. This requires assumptions on cell size, cell shape and carbon content per biovolume (Tarran et al., 2006). Another alternative is to derive biovolume from scattering properties of the cell using a pulse shape recording flowcytometer as used in this study. This relationship appears to be taxon-specific (Rijkeboer, pers. comm.) and needs to be further explored by comparison of calculated biovolume (based on the Image in Flow pictures) and the flowcytometric properties of the cell. The FRRf offers the possibility to circumvent the use of phytoplankton biomass as a necessary parameter to estimate primary productivity altogether by estimating the amount of Photosystem II Reaction Centers or total absorption by the PSII concentration (i.e. a_{LHII}; Oxborough et al., 2012). As long as there is no uncontroversial method to derive phytoplankton biomass, calculation of multiple parameters and critical evaluation remains necessary.

The FCM was able to visualize the spatial variability of the phytoplankton community in the Dutch North Sea. The typical spring bloom was partly captured during the cruise of April, with high total fluorescence and high relative abundance of micro- and nanophytoplankton in comparison to other months. In contrast, in August the community was dominated by picophytoplankton with only sporadic observations of microphytoplankton. In addition, spatial variability in size distribution was clearly visible as a stronger presence of microphytoplankton in coastal regions than offshore. Microphytoplankton are a better food source for higher trophic levels than picophytoplankton. Picophytoplankton is part of the microbial food web, with less trophic efficiency and low contribution to carbon export (Azam et al., 1983; Finkel et al., 2010). The shift from nanophytoplankton-dominated communities in April to picophytoplankton-dominated communities in August therefore implicates that over the year the tropic efficiency and carbon export decrease. These spatial and temporal changes are a yearly phenomenon, influenced by the strong seasonal dynamics in the Dutch North Sea that affects the spatial distribution and community composition of the phytoplankton community (Baretta-Bekker et al., 2009; Brandsma et al., 2011). It is important to monitor interannual variability over the years to monitor changes in biogeochemical cycles and the carrying capacity of the ecosystem. To increase the informational value of the flowcytometry data beyond size, the FCM clusters would need to reflect taxonomic or functionally relevant groups. Interesting groups include calcifiers, silicifiers, DMS producers (such as *Phaeocystis*) or nitrogen fixers (le Quéré et al., 2005). The lack of identification of distinct clusters makes this so far impossible, although some species are recognizable as *Phaeocystis* sp. (Rijkeboer, unpublished). Marrec et al. (2018) manually separated up to 10 phytoplankton groups from the data of the Cytosense flowcytometer. Yet, most of these groups comprise many taxonomic genera and, apart from the size or pigment composition, hindering further interpretation of their role in the ecosystem or biogeochemical cycles. However, the distinction between different pigment groups can provide useful information on food web functioning. Chlorophyll-*c* containing algae (Chromista) contain long-chained essential fatty acids like docosahexaenoic acid (DHA) and eicosapenthic acid (EPA) which are lacking in green algae (some Prasinophycaea excepted) or cyanobacteria (Dijkman and Kromkamp, 2006). Thus, information about food quality can be obtained from FCM. For detection of nuisance phytoplankton, distinct clusters are lacking. Yet, toxicity in phytoplankton can differ even between strains within one species, so finding a distinct cluster by flowcytometry is challenging (Tillman and Rick, 2003). However, the identification of 'suspicious' clusters with potential toxic species could already be helpful. These suspicious clusters can flag sampling points to be further inspected by a specialist using microscopy.

Monitoring of the photophysiology of the phytoplankton by FRR fluorometry can supplement the flowcytometry measurements. For instance, the hypothesized spring bloom detected by the flowcytometer in April is confirmed by photophysiological parameters;

photophysiology was uniform and primary productivity high. Between April and May, the efficiency of PSII (F_v/F_m; Fig. 4) decreased throughout the Dutch North Sea. A decreasing F_v/F_m is generally associated with limiting nutrient conditions or other abiotic, but can also reflect a change in community composition stressors (Suggett et al., 2009b; Kolber et al. 1988; Kolber and Falkowski, 1993; Beardall et al. 2001; Ly et al. 2014). Photophysiological parameters vary per taxonomic group; smaller taxa typically have lower F_v/F_m values and higher σ_{PSII} values (Kolber et al., 1988; Suggett et al., 2009b). No major shift in community composition was identified by flowcytometry between April and May. This suggests that an abiotic stressor, such as the nutrient limiting conditions in a large part of the Dutch North Sea, instead of the community composition was driving the decrease in efficiency of PSII. In contrast, the recovery of the F_v/F_m between May and June did coincide with a shift in community composition. In May the phytoplankton communities were mostly nanophytoplankton-dominated, while in June the communities were dominated by picophytoplankton (offshore) and microphytoplankton (coastal). So, although recovery of the F_v/F_m can also occur as an adaptation of the phytoplankton to nutrient limiting conditions (Kruskopf and Flynn, 2005), it seems that the shift in community composition was the major driver for the recovery of the F_v/F_m between May and June. These findings are a good example of how concurrent measurements by flowcytometry and Fast Repetition Rate fluorometry can supplementary improve ecosystem understanding. When including photophysiology (or photophysiology based GPP estimates) in a monitoring program, it is critical to consider methodological constraints (Hughes et al., 2018). For instance at low phytoplankton abundance, the fluorescence signal becomes too noisy for calculation of parameters. Moreover, blank correction is essential for retrieving accurate FRRf data (Cullen and Davis, 2003). FRRf measurements are affected by the interference of colored dissolved matter which can lead to under or overestimation of some parameters (like F_v/F_m; Cullen and Davis, 2003). The blank correction is a manual measurement and should be done regularly and at least when abiotic conditions change (Hughes et al., 2018). For monitoring purposes, it is important to take into account diurnal variability. Diurnal trends make extrapolation to daily rates challenging. Most photophysiological parameters we measured showed diurnal trends (Fig. 5). The diurnal trend is dictated by the phytoplankton cell cycle, a circadian oscillator and photophysiological response to varying irradiance (Suzuki and Johnson, 2001; Cohen and Golden, 2015; Schuback et al., 2016). Phytoplankton use photophysiological plasticity to minimize photodamage and optimize growth under fluctuating irradiance (Schuback et al., 2016; Behrenfeld et al., 2002). The electron requirement for carbon fixation is also subject to diurnal variation (Schuback et al., 2016; Lawrenz et al., 2013; Raateoja, 2004). To interpret spatial variability separately from temporal variability and to provide a more reliable estimate of gross primary productivity, Schuback et al. (2016) suggest a correction with normalized Stern-Volmer quenching (NPQ_{NSV}). This approach needs further research, for example by using a Lagrangian approach where the photosynthetic activity of the same population is followed during the day. Until a reliable correction method has been established, a monitoring program including photophysiology should account for diurnal variability, for instance by using only measurements collected in a certain timeframe or from buoys. Despite the limitations of GPP estimates by variable fluorescence, our results clearly show large spatial variability in gross primary production that is not explained by diurnal variability. This spatial heterogeneity is not fully captured by sampling at the standard low-resolution monitoring stations, showing the added value of our approach.

Phytoplankton biomass does not necessarily reflect primary productivity, as high grazing pressure can keep biomass low while production is high. This is clearly visualized by the lack of resemblance between patterns in cell numbers (Fig. 3 a-d) and gross primary productivity (Fig. 6). Gross primary productivity estimates by FRR fluorometry are based on measurements of the first step of photosynthesis; the efficiency at which photons are captured and electrons transferred. However, to interpret gross primary productivity in an ecological or biogeochemical meaningful way, the FRR units of electrons per unit time need to be converted to carbon units. In general, gross photosynthesis correlates well with photosynthetic oxygen evolution (Suggett et al., 2003), and multiple studies have shown a good correlation between 14C-derived estimates of primary productivity and FRRf-derived estimates using a constant conversion factor (Melrose et al., 2006; Kromkamp et al., 2008). However, in reality, this parameter is not a constant, as along the pathway from electron to carbon atom electrons are consumed by other cell processes (Flameling and Kromkamp, 1998; Halsey and Jones, 2015; Schuback et al., 2016). As the cell processes from photon absorbance to carbon

assimilation are known to vary with abiotic conditions, we expect that identification of biogeographic regions can aid in predicting regional Φe,C (Lawrenz et al., 2013). Calibration with other methods, such as concurrent C14 of C13 incubations, could help to better understand the processes from electron excitation to carbon fixation. However, these methods introduce other uncertainties; they measure a productivity in between net and gross primary productivity, depending on the incubation time and growth rate of the phytoplankton (Halsey and Jones, 2015). For now, a reliable GPP estimate in carbon units from FRR fluorometry requires more research and estimates provide relative rather than qualitative values. Despite its limitations, the ability to study life phytoplankton rates without long-term incubation effects, makes the method promising. Additionally, the high sampling resolution allows for identification of extra sampling points based on real-time projections, opening up early warning methodologies. For example, in the April cruise both Noordwijk 70 and Terschelling 235 km show high gross primary productivity, but in between both high and low productivity rates occur which are not detected with the current sampling program (Fig. 6). Extrapolation of surface measurements to water column estimates is required to assess the carrying capacity of the ecosystem and the contributions to biogeochemical cycles. Surface water measurements are only a good reflection of the water column when mixed layer depth is deeper than the euphotic zone. Stratification or mixed layer depth shallower than the euphotic zone can result in subsurface chlorophyll maximum layers and significantly different phytoplankton community (Latasa et al., 2017). Only frequent CTD casts equipped with PAR sensor can determine the vertical heterogeneity, mixed layer depth and the light extinction in the water column.

High-resolution methods such as the FRRf and the flowcytometer result in a multitude of parameters. Cluster methods can be helpful in bringing together these parameters for interpretation. The spectral clustering method used in this study was originally designed to detect phytoplankton blooms and understanding the involved dynamics (Rousseeuw et al., 2015; Lefebvre and Poisson-Caillault, 2019). This spectral cluster analysis on parameters from the FRRf and the flowcytometer allowed for the identification of distinct phytoplankton communities or biogeographic regions that differed per cruise. A clear distinction between phytoplankton communities of the coastal zone and offshore regions could be made in all months, except May. In two cruises, in April and June, it was indeed possible to identify regions with distinct phytoplankton communities. During the cruise in May, the clustering did not result in clear mesoscale patterns but was heterogeneous over the whole Dutch North Sea. Unfortunately, the model was not able to visualize all spatial heterogeneity. For instance, in April off the coast from Terschelling a distinct community with a high abundance of phycoerythrin-containing taxa did not result in a separate cluster. Additionally, temporal variation (i.e. day-night differences) was interfering with the spatial clustering in August. So, although such models are useful for visualization and following changes in spatial heterogeneity, input and output need to be critically evaluated before implementation in monitoring programs. To test whether the differences between months result from seasonal variation or other factors, results over multiple years and additional seasonal cruises need to be made to better characterize the heterogeneity of the phytoplankton community structure.

The purpose of a phytoplankton monitoring program is to monitor the presence of functional types of phytoplankton, including the harmful taxa, the carrying capacity of the ecosystem and changes in biogeochemical cycling. The objective of this study was to evaluate the use of FRR fluorometry and flowcytometry for such monitoring purposes. The four conducted cruises spread over 5 months offered a wide variety of environmental conditions and phytoplankton community states, which the utilized methods were able to visualize. Inclusion of high-resolution methods in monitoring programs allows for analysis of finer scale events. Furthermore, it allows for analysis of living phytoplankton and is thereby able to measure rates and avoid effects of preservation and storage of samples. Another advantage is that high-resolution methods allow for easier comparison between countries, once common protocols are established. Nevertheless, low-resolution methods remain a necessity for more detailed taxonomic analysis, extrapolation over the entire water column, to calibrate and to correct for blanks. Data analysis is a challenge when implementing high-resolution methods, where cluster methods could simplify and standardize analysis. The cluster analysis of flowcytometric data has potential for improvement to increase the informative value of the method. Especially identification of phytoplankton clusters with a functional quality, such as nitrogen fixers, calcifiers, DMS-producers or clusters with high food quality, would be helpful for

interpretation of ecosystem dynamics and biogeochemical fluxes. Regarding the FRRf, the main challenge is converting the electron transport rate to gross primary productivity in carbon units. Further research in these topics would benefit the implementation of these methods into monitoring protocols. Furthermore, it is important to account for diurnal patterns in monitoring set-up to be able to distinguish between diurnal and spatial variability. Possibly the diurnal variability could be modeled, but more studies with a Langragian based approach are needed for a better understanding of the impact of diurnal variability in the data. The combination of high-resolution in situ methods with remote sensing has the potential to further increase the spatial and temporal scale. Estimating biological parameters using remote sensing is challenging, especially in turbid, case-2 waters (Gohin et al., 2005; van der Woerd et al., 2008). Therefore, *in vivo* measurements are required to calibrate remote sensing based models and we suggest that automated flowcytometry and production measurements based on FRRf methodology can fulfill this role. Overall, our proposed high-resolution measurement set-up has the potential to improve phytoplankton monitoring by supplementing existing low-resolution monitoring programs.

Acknowledgements

We want to thank the captain and crew of the RV *Zirfaea* and the shipboard Eurofins employees for their hospitality and great help during the cruises. We thank Annette Wielemaker for assistance with the GIS maps of primary production, René Geertsema for assistance with the flowcytometry data analysis and Ralf Schiebel for useful comments on the manuscript. Furthermore, we would like to thank the Rijkswaterstaat laboratory for conducting the nutrients and chlorophyll measurements and Rijkswaterstaat for the opportunity to perform measurements alongside the regular monitoring program. This project has received funding from the European Union's Horizon 2020 research and innovation programme under grant agreement No 654410 (Jerico-Next).

References

Alvarez-Fernandez, S., and Riegman, R.: Chlorophyll in North Sea coastal and offshore waters does not reflect long term trends of phytoplankton biomass, J. of Sea Res., 91, 35–44, doi: 10.1016/j.seares.2014.04.005, **2014.**

Azam, F., Fenchel, T., Field, J., Gray, J., Meyer-Reil, L., and Thingstad, F.: The Ecological Role of Water-Column Microbes in the Sea, Mar. Ecol. Prog. Ser., 10(3), 257-263, **1983.**

Baretta-Bekker, J. G., Baretta, J. W., Latuhihin, M. J., Desmit, X., and Prins, T. C.: Description of the long-term (1991-2005) temporal and spatial distribution of phytoplankton carbon biomass in the Dutch North Sea, J. of Sea Res., 61(1–2), 50–59. doi:10.1016/j.seares.2008.10.007, **2009.**

Beardall, J., Berman, T., Heraud, P., Kadiri, M. O., Light, B. R., Patterson, G., Roberts, S., Sulzberger, B., Sahan, E., Uehlinger, U., and Wood, B.: A comparison of methods for detection of phosphate limitation in microalgae, Aquat. Sci., 63, 107-121. **2001.**

Behrenfeld, M. J., Maranon, E., Siegel, D. A., and Hooker, S. B.: Photoacclimation and nutrient-based model of light-saturated photosynthesis for quantifying oceanic primary production, Mar. Ecol. Prog. Ser., 228, 103-117, **2002.**

Behrenfeld, M. J., O'Malley, R. T., Siegel, D. A., McClain, C. R., Sarmiento, J. L., Feldman, G. C., Milligan, A. J., Falkowski, P. G., Letelier, R. M., and Boss, E. S.: Climate-driven trends in contemporary ocean productivity, Nature, 444, 7120, 752–755, doi:10.1038/nature05317, **2006.**

5 Brandsma, J., Hopmans, E. C., Philippart, C. J. M., Veldhuis, M. J. W., Schouten, S., Sinninghe Damsté, J. S.: Low temporal variation in the intact polar lipid composition of North Sea coastal marine water reveals limited chemotaxonomic value, Biogeosciences, 9, 3, 1073–1084. doi:10.5194/bg-9-1073-2012, **2011.**

Burson, A., Stomp, M., Akil, L., Brussaard, C. P. D., and Huisman, J.: Unbalanced reduction of nutrient loads has created an offshore
10 gradient from phosphorus to nitrogen limitation in the North Sea, Limnol. Oceanogr., 61, 869–888, doi:10.1002/lno.10257, **2016.**

Capuzzo, E., Stephens, D., Silva, T., Barry, J., Forster, R. M.: Decrease in water clarity of the southern and central North Sea during the 20th century. Glob. Change Biol., 21, 6, 2206–2214, doi:10.1111/gcb.12854, **2015.**

15 Capuzzo, E., Lynam, C. P., Barry, J., Stephens, D., Forster, R. M., Greenwood, N., McQuatters-Gollop, A., Silva, T., van Leeuwen, S.M. and Engelhard, G. H.: A decline in primary production in the North Sea over 25 years, associated with reductions in zooplankton abundance and fish stock recruitment, Glob. Change Biol., 1–13, doi:10.1111/gcb.13916, **2017.**

Cloern, J. E., Foster, S. Q. and Kleckner, A. E.: Phytoplankton primary production in the world's estuarine-coastal ecosystems,
20 Biogeosciences, 11, 9, 2477–2501, doi:10.5194/bg-11-2477-2014, **2014.**

Cohen, S. E. and Golden, S. S.: Circadian Rhythms in Cyanobacteria, Microbiol. Mol. Biol. Rev., 79, 4, 373-85, doi:10.1128/MMBR.00036-15, **2015.**

25 Cullen, J. J., and Davis, R. F.: The blank can make a big difference in oceanographic measurements. Limnol. Oceanogr. Bulletin, 12, 2, 29–35, **2001.**

Dijkman, N. A. and Kromkamp, J.C. Phospholipid-derived fatty acids as chemotaxonomic markers fro phytoplankton: application for inferring phytoplankton composition. Mar. Ecol. Progr. Ser. 424, 113-125, **2006**

30

Falkowski, P. and Kiefer, D. A.: Chlorophyll *a* fluorescence in phytoplankton: relationship to photosynthesis and biomass, J. Plankton Res., 7, 5, 715–731, **1985.**

Falkowski, P.G.: Biogeochemical Controls and Feedbacks on Ocean Primary Production, Science, 281, 5374, 200–206,
35 doi:10.1126/science.281.5374.200, **1998.**

Finkel, Z. V., Beardall, J., Flynn, K. J., Quigg, A., Rees, T. A. V., and Raven, J. A.: Phytoplankton in a changing world: cell size and elemental stoichiometry, J. Plankton Res., 32, 1, 119–137, doi:10.1093/plankt/fbp098, **2010.**

40 Flameling, I.A. and Kromkamp, J.C.: Light dependence of quantum yields for PSII charge separation and oxygen evolution in eukaryotic algae, Limnol. Oceanogr., 43, 284-297, **1998.**

Flynn, K. J.: Algal carbon-nitrogen metabolism: a biochemical basis for modelling the interactions between nitrate and ammonium uptake, J. Plankton.Res., 13, 373-387, **1991.**

Flynn, K.J.: Modelling marine phytoplankton growth under eutrophic conditions, J. of Sea Res., 54, 92-103, **2005.**

5

Franck, F., Juneau, P., and Popovic, R.: Resolution of the Photosystem I and Photosystem II contributions to chlorophyll fluorescence of intact leaves at room temperature, BBA-Bioenergetics, 1556, 2–3, 239–246, doi:10.1016/S0005-2728(02)00366-3, **2002.**

10 Geider, R. J., MacIntyre, H. L., and Kana, T. M.: Dynamic model of phytoplankton growth and acclimation: responses of the balanced growth rate and the chlorophyll *a*:carbon ratio to light, nutrient-limitation and temperature, Mar. Ecol. Prog. Ser., 148, 187-200, **1997.**

Giannini, M. F. C., and Ciotti, Á. M.: Parameterization of natural phytoplankton photo-physiology: Effects of cell size and nutrient
15 concentration, Limnol. Oceanogr., 61, 4, 1495–1512, doi:10.1002/lno.10317, **2016.**

Gohin, F., Loyer, S., Lunven, M., Labry, C., Froidefond, .J.-M., Delmas, D., Huret, M. and Herbland. A.: Satellite-derived parameters for biological modelling in coastal waters: Illustration over the eastern continental shelf of the Bay of Biscay, Remote Sens. Environ., 95, 29-46, **2005.**

20

Goss, R., Ann Pinto, E., Wilhelm, C., and Richter, M.: The importance of a highly active and ΔpH-regulated diatoxanthin epoxidase for the regulation of the PS II antenna function in diadinoxanthin cycle containing algae, J. Plant Physiol., 163, 10, 1008–1021, doi:10.1016/j.jplph.2005.09.008, **2006.**

25 Halsey, K. H., and Jones, B. M.: Phytoplankton Strategies for Photosynthetic Energy Allocation. Annu. Rev. Mar. Sci., 7, 265–97, doi:10.1146/annurev-marine-010814-015813, **2015.**

Hughes, D. J., Campbell, D. A., Doblin, M. A., Kromkamp, J. C., Lawrenz, E., Moore, C.M., Oxborough, K., Prášil, O., Ralph, P. J., Alvarez,M.F., Suggett, D. J.: Roadmaps and Detours : Active Chlorophyll - *a* Assessments of Primary Productivity Across Marine
30 and Freshwater Systems. Environ. Sci. Technol. 2018, 52, 12039−12054, doi:10.1021/acs.est.8b03488, **2018.**

Kassambara, A. and Mundt, F.: factoextra: Extract and Visualize the Results of Multivariate Data Analyses. R package version 1.0.5. https://CRAN.R-project.org/package=factoextra, **2017.**

35 Kolber, Z., Zehr, J., and Falkowski, P.G.: Effects of growth irradiance and nitrogen limitation on photosynthetic energy conversion in photosystem II, Plant Physiology, 88, 923-929, **1988.**

Kolber, Z. and Falkowski, P. G.: Use of active fluorescence to estimate phytoplankton photosynthesis in situ, Limnol. Oceanogr., 38, 1646-1665, **1993.**

40

Kolber, Z. S., Prášil, O., and Falkowski, P. G.: Measurements of variable chlorophyll fluorescence using fast repetition rate techniques: Defining methodology and experimental protocols, BBA-Bioenergetics, 1367, 1–3, 88–106, doi:10.1016/S0005-2728(98)00135-2, **1998.**

Kromkamp, J. C., and Forster, R. M.: The use of variable fluorescence measurements in aquatic ecosystems: differences between multiple and single turnover measuring protocols and suggested terminology, Eur. J. Phycol., 38, 2, 103–112, doi:10.1080/0967026031000094094, **2003.**

5

Kromkamp, J. C., Dijkman, N. A., Peene, J., Simis, S. G. H., and Gons, H. J.: Estimating phytoplankton primary production in Lake IJsselmeer (The Netherlands) using variable fluorescence (PAM-FRRF) and C-uptake techniques Estimating phytoplankton primary production in Lake IJsselmeer (The Netherlands) using variable fluoresce, Eur. J. Phycol., 262, doi:10.1080/09670260802080895, **2008.**

10

Kromkamp, J.C., and Van Engeland, T.: Changes in phytoplankton biomass in the western Scheldt estuary during the period 1978-2006, Estuaries Coasts, 33, 2, 270–285, doi:10.1007/s12237-009-9215-3, **2010.**

Kruskopf, M. and Flynn, K.J.: Chlorophyll content and fluorescence responses cannot be used to gauge reliably phytoplankton
15 biomass, nutrient status or growth rate, New Phytol., 169, 525-536, **2005.**

Latasa, M., Cabello, A. M., Morán, X. A. G., Massana, R. and Scharek, R.: Distribution of phytoplankton groups within the deep chlorophyll maximum, Limnol. Oceanogr., 62, 665-685, **2017.**

20 Lawrenz, E., Silsbe, G., Capuzzo, E., Ylöstalo, P., Forster, R. M., Simis, S. G. H., Prášil, O., Kromkamp, J. C., Hickman, A. E., Moore, C. M., Forget, M. H., Geider, R. J., and Suggett, D. J.: Predicting the Electron Requirement for Carbon Fixation in Seas and Oceans, PLoS ONE, 8, 3, doi:10.1371/journal.pone.0058137, **2013.**

Lefebvre, A., and Poisson-Caillault, E.: High resolution overview of phytoplankton spectral groups and hydrological conditions in
25 the eastern English Channel using unsupervised clustering. Mar. Ecol. Prog. Ser., doi:10.3354/meps12781, **2019.**

Ly, J., Philippart, C. J. M., and Kromkamp, J.C.: Phosphorus limitation during a phytoplankton spring bloom in the western Dutch Wadden Sea, J. of Sea Res., 88, 109-120, **2014.**

30 Marinov, I., Doney, S. C., and Lima, I. D.: Response of ocean phytoplankton community structure to climate change over the 21st century: partitioning the effects of nutrients, temperature and light, Biogeosciences, 7, 12, 3941–3959. doi:10.5194/bg-7-3941-2010, **2010.**

Marrec, P., Doglioli, A. M., Grégori, G., Dugenne, M., Della Penna, A., Bhairy, N., Cariou, T., Hélias Nunige, S., Lahbib, S.,
35 Rougier, G., Wagener, T., and Thyssen, M.: Coupling physics and biogeochemistry thanks to high resolution observations of the phytoplankton community structure in the North-Western Mediterranean Sea, Biogeosciences Discussions, 1–54, doi:10.5194/bg-2017-343, **2017.**

Melrose, D. C., Oviatt, C. A., O'Reilly, J. E., and Berman, M. S.: Comparisons of fast repetition rate fluorescence estimated primary
40 production and 14C uptake by phytoplankton, Mar. Ecol. Prog. Ser., 311, 37–46, doi:10.3354/meps311037, **2006.**

Montes-Hugo, M., Doney, S. C., Ducklow, H. W., Fraser, W., Martinson, D., Stammerjohn, S. E., and Schofield, O.: Recent Changes in Phytoplankton Communities Associated with Rapid Regional Climate Change Along the Western Antarctic Peninsula, Science, 323, 5920, 1470–1473, doi:10.1126/science.1164533, **2009.**

Moore, C. M., Suggett, D. J., Hickman, A. E., Kim, Y.-N., Tweddle, J. F., Sharples, J., Geider, R.J., and Holligan, P. M.: Phytoplankton photoacclimation and photoadaptation in response to environmental gradients in a shelf sea, Limnol. Oceanogr. 44, 0, 1–46, doi:10.4319/lo.2006.51.2.0936, **2006.**

Oxborough, K., Moore, C. M., Suggett, D. J., Lawson, T., Chan, H. G., and Geider, R. J.: Direct estimation of functional PSII reaction center concentration and PSII electron flux on a volume basis : a new approach to the analysis of Fast Repetition Rate fluorometry (FRRf) data, Oceanography.:methods, 142–154. doi:10.4319/lom.2012.10.142, **2012.**

Peeters, J., and Peperzak, L.: Nutrient limitation in the North Sea: a bioassay approach, Neth. J. Sea Res., 26, 1, 61–73, doi:10.1016/0077-7579(90)90056-M, **1990.**

Philippart, C. J. M., Cade, G. C., Raaphorst, W. van, and Riegman, R.: Long-term phytoplankton – nutrient interactions in a shallow coastal sea: Algal community structure, nutrient budgets, and denitrification potential, Limnol. Oceanogr., 45, 1, 131–144, **2000.**

Philippart, C. J. M., Beukema, J. J., Cadée, G. C., Dekker, R., Goedhart, P. W., Van Iperen, J. M., Leopold, M. F. Herman, P. M. J.: Impacts of nutrient reduction on coastal communities, Ecosystems, 10, 1, 95–118, doi:10.1007/s10021-006-9006-7, **2007.**

Philippart, C. J. M., Anadón, R., Danovaro, R., Dippner, J. W., Drinkwater, K. F., Hawkins, S. J., Oguz, T., O'Sullivan, G., Reid, P. C. (2011). Impacts of climate change on European marine ecosystems: Observations, expectations and indicators, J. Exp. Mar. Biol. Ecol., 400, 1–2, 52–69, doi:10.1016/j.jembe.2011.02.023, **2011.**

Poisson-caillault, E. and Ternynck, P.: uHMM: Construct an Unsupervised Hidden Markov Model. R Package version 1.0, https://cran.r-project.org/package=uhmm, **2016.**

Quéré, C. Le, Harrison, S. P., Colin Prentice, I., Buitenhuis, E. T., Aumont, O., Bopp, L., Claustre, H., Cotrim Da Cunha, L., Geider, R.J., Giraud, X., Klaas, C., Kohfeld, K.E., Legendre, L., Manizza, M., Platt, T., Rivkin, R.B., Sathyendranath, S., Uitz, J., Watson, A.J., and Wolf-Gladrow, D.: Ecosystem dynamics based on plankton functional types for global ocean biogeochemistry models, Global Change Biol., 11, 11, 2016–2040, doi:10.1111/j.1365-2486.2005.01004.x, **2005.**

Raateoja, M. P.: Fast repetition rate fluorometry (FRRF) measuring phytoplankton productivity: A case study at the entrance to the Gulf of Finland, Baltic Sea, Boreal Env. Res., 9, 263–276, **2004.**

Rantajärvi, E., Olsonen, R., Hällfors, S., Leppänen, J. M., and Raateoja, M.: Effect of sampling frequency on detection of natural variability in phytoplankton: Unattended high-frequency measurements on board ferries in the Baltic Sea, ICES J. Mar. Science, 55, 4, 697–704. doi:10.1006/jmsc.1998.0384, **1998.**

Rijkeboer, M.: Automated characterization of phytoplankton community into size and pigment groups based on flow cytometry, MEM 2018-20, RWS Information, 18, **2018.**

Rousseeuw, K., Poison Caillault, E., Lefebvre, A., Hamad, D.: Achimer Hybrid hidden Markov model for marine environment monitoring, IEEE J-STARS, 8, 1, 204–213, doi:10.1109/JSTARS.2014.2341219, **2015.**

Rutten, T.: Evaluatie testen van diverse CytoSense configuraties, TRP2015.001, **2015.**

Sarmiento, J. L., Slater, R., Barber, R., Bopp, L., Doney, S. C., Hirst, A. C., Kleypas, J., Matear, R., Mikolajewicz, U., Monfray, P., Soldatov, V., Spall, S. A., and Stouffer, R.: Response of ocean ecosystems to climate warming, Global Biogeochem. Cy., 18, 3, GB3003, doi:10.1029/2003GB002134, **2004.**

Schiebel, R., Spielhagen, R. F., Garnier, J., Hagemann, J., Howa, H., Jentzen, A., Martínez-Garcia, A., Meiland, J., Michel, E., Repschläger, J., Salter, I., Yamasaki, M., and Haug, G.: Modern planktic foraminifers in the high-latitude ocean, Mar. Micropaleontol., 136, 1–13, doi:10.1016/j.marmicro.2017.08.004, **2017.**

Seadatanet: SeaDataCloud Flow Cytometry Standardised Cluster Names, Natural Environment Research Council, Version 3, http://vocab.nerc.ac.uk/collection/F02/current/F0200007/, **2018.**

Sieburth J. M., Smetacek, V., and Lenz, J.: Pelagic ecosystem structure: heterotrophic compartments of the plankton and their relationship to plankton size fractions, Limnol. Oceanogr., 23, 1256–1263, **1978.**

Schuback, N., Flecken, M., Maldonado, M. T., Tortell, P. D. (2016). Diurnal variation in the coupling of photosynthetic electron transport and carbon fixation in iron-limited phytoplankton in the NE subarctic Pacific, Biogeosciences, 13, 4, 1019–1035, doi:10.5194/bg-13-1019-2016, **2016.**

Sündermann, J., and Pohlmann, T.: A brief analysis of North Sea physics, Oceanologia, 53, 3, 663–689, doi:10.5697/oc.53-3.663, **2011.**

Silsbe, G.M. and Kromkamp, J.C.: Modeling the irradiance dependency of the quantum efficiency of photosynthesis, Limnol. Oceanogr.: Methods, 10, 9, 645–652. doi:10.4319/lom.2012.10.645, **2012.**

Silsbe, G.M., Oxborough, K., Suggett, D.J., Forster, R.M., Ihnken, S., Komárek, O., Lawrenz E., Prášil, O., Röttgers, R., Šicner, M., Simis, S.G.H., Van Dijk, M., Kromkamp, J.C.: Toward autonomous measurements of photosynthetic electron transport rates: An evaluation of active fluorescence-based measurements of photochemistry, Limnol. Oceanogr.: Methods, 13, 3, 138–155, doi:10.1002/lom3.10014, **2015.**

Silsbe, G.M., Behrenfeld, M.J., Halsey, K.H., Milligan, A.J., Westberry, T.K.: The CAFE model: A net production model for global ocean phytoplankton, Global Biogeochem. Cy., 30, 12, 1756–1777, doi:10.1002/2016GB005521, **2016.**

Smyth, T.J., Pemberton, K.L., Aiken, J., Geider, R.J.: A methodology to determine primary production and phytoplankton photosynthetic parameters from Fast Repetition Rate Fluorometry, J. Plankton Res., 26, 11, 1337–1350, doi:10.1093/plankt/fbh124**, 2004.**

Suggett, D. J., Oxborough, K., Baker, N. R., MacIntyre, H. L., Kana, T. M., Geider, R .J.: Fluorescence Measurements for Assessment of Photosynthetic Electron Transport in Marine Phytoplankton, Eur. J. Phycol., 38, 4, 371–384, doi:10.1080/0967026031000161265, **2003.**

Suggett, D. J., MacIntyre, H. L., Kana, T. M., Geider, R. J.: Comparing electron transport with gas exchange: Parameterising exchange rates between alternative photosynthetic currencies for eukaryotic phytoplankton, Aquat. Microb. Ecol., 56, 2–3, 147–162, doi:10.3354/ame01303, **2009a.**

Suggett, D.J., Moore, C. M., Hickman, A. E., and R.J. Geider, R. J.: Interpretation of fast repetition rate (FRR) fluorescence: signatures of phytoplankton community structure versus physiological state, Mar. Ecol. Prog. Ser., 376, 1-19, **2009b.**

Suzuki, L., and Johnson, C. H.: Algae Know the Time of Day: Circadian and Photoperiodic Programs, J. Phycol., 37, 933–942, **2001.**

Stolte, W., and Riegman, R.: Effect of phytoplankton cell size on transient- state nitrate and ammonium uptake kinetics, Microbiology, 141, 1221–1229, **1995.**

Sündermann, J., and Pohlmann, T.: A brief analysis of North Sea physics, Oceanologia, 53, 3, 663–689, doi:10.5697/oc.53-3.663, **2011.**

Tarran, G. A., Heywood, J. L., and Zubkov, M. V.: Latitudinal changes in the standing stocks of nano- and picoeukaryotic phytoplankton in the Atlantic Ocean, Deep-Sea Res. Pt II, 53, 14–16, 1516–1529, doi:10.1016/j.dsr2.2006.05.004, **2006.**

Thyssen, M., Alvain, S., Dessailly, D., Rijkeboer, M., Guiselin, N., Creach,: High-resolution analysis of a North Sea phytoplankton community structure based on in situ flow cytometry observations and potential implication for remote sensing, Biogeosciences, 12, 4051–4066, doi:10.5194/bg-12-4051-2015, **2015.**

Tillmann, U., and Rick, H. J.: North Sea phytoplankton: A review. Senckenbergiana Maritima, 33, 1–2, 1–69, doi:10.1007/BF03043047, **2003.**

Van der Woerd, H. J. And Pasterkamp, R.: HYDROPT: A fast and flexible method to retrieve chlorophyll-a from multispectral satellite observations of optically complex coastal waters, Remote Sens. Environ., 112, 1795-1807, **2008.**

Vaulot, D., Eikrem W., Viprey, M., and Moreau, H.: The diversity of small eukaryotic phytoplankton (< or =3 micron) in marine ecosystems, FEMS Microbiol. Rev., 32, 795–820, **2008.**

Webb, W. L., Newton, M., and Starr, D.: Carbon dioxide exchange of *Alnus rubra*: a mathematical model, Oecologia, 17, 281-291, **1974.**

Wickham, H.: ggplot2: Elegant Graphics for Data Analysis, Springer-Verlag, New York, **2009.**

Zuur, A.F., Ieno, E.N., Walker, N., Saveliev, A.A., and Smith, G.M.: Mixed effects models and extensions in ecology with R, Springer, **2009.**